PCCP

PAPER

View Article Online
View Journal | View Issue

Cite this: *Phys. Chem. Chem. Phys.*, 2014, **16**, 20780

BaC: a thermodynamically stable layered superconductor

Dian-Hui Wang,[a] Huai-Ying Zhou,[ab] Chao-Hao Hu,*[bc] Artem R. Oganov,[def] Yan Zhong[b] and Guang-Hui Rao[b]

Received 25th June 2014,
Accepted 15th August 2014

DOI: 10.1039/c4cp02781g

www.rsc.org/pccp

To predict all stable compounds in the Ba–C system, we perform a comprehensive study using first-principles variable-composition evolutionary algorithm USPEX. We find that at 0 K the well-known compound BaC_2 is metastable in the whole pressure range 0–40 GPa, while intercalated graphite phase BaC_6 is stable at 0–19 GPa. A hitherto unknown layered orthorhombic *Pbam* phase of BaC has structure consisting of alternating layers of Ba atoms and layers of stoichiometry Ba_2C_3 containing linear C_3 groups and is predicted to be stable in the pressure range 3–32 GPa. From our electron–phonon coupling calculations, the newly found BaC compound is a phonon-mediated superconductor and has a critical superconductivity temperature T_c of 4.32 K at 5 GPa. This compound is dynamically stable at 0 GPa and therefore may be quenchable under normal conditions.

Introduction

Metal carbides have attracted much attention due to their interesting physical and chemical properties. For example, superconductivity has been found in the intercalated graphite compounds, such as CaC_6 (T_c = 11.5 K)[1] and YbC_6 (T_c = 6.5 K),[2] and in some metal dicarbides such as YC_2 (T_c = 4.02 K)[3] and LaC_2 (T_c = 1.8 K).[4] The first reported superconducting alkali metal-graphite intercalation compound is KC_8 with a T_c = 0.14 K.[5] However, upon increasing the alkali metal concentration *via* a high-pressure fabrication technique, the transition temperature T_c can be further increased up to 1.9 K in LiC_2[6] and 5 K in NaC_2.[7] In the graphite intercalation compounds, the interlayer state is also found to be occupied and the energy of the interlayer band is controlled by a combination of its occupancy and the separation between the carbon layers.[8] These covalently bonded carbon-based materials often have strong electron–phonon coupling and phonon frequencies[9] and therefore can be superconducting when they have finite density of states at the Fermi level.

In the Ba–C system, only two carbides are known – dicarbide BaC_2 and the intercalated graphite BaC_6. Under ambient conditions, BaC_2 crystallizing in the CaC_2-type structure with space group *I*4/*mmm* can be considered as a tetragonally distorted NaCl-type arrangement in which Ba atoms occupy the Na sites and characteristic C_2 dumbbells on the Cl sites. Recently, pressure-induced structural transition of BaC_2 has been studied by synchrotron X-ray diffraction and Raman spectroscopy at room temperature. It was found that the *I*4/*mmm* phase of BaC_2 transforms into an $R\bar{3}m$ rhombohedral structure at 4 GPa and amorphization takes place above 30 GPa.[10] Calculations within density functional theory (DFT) indicate that the *I*4/*mmm* BaC_2 is an insulator with a DFT band gap of about 2.2 eV.[11] BaC_6, unlike YbC_6 and CaC_6, shows no trace of superconductivity even at a very low temperature down to 80 mK, because the separation between graphene layers in BaC_6 is so large that superconductivity is suppressed.[12]

It is well known that pressure, as one of the fundamental thermodynamic variables, can drastically alter the chemical and physical properties of materials and give rise to a large number of novel phenomena which only emerge under high-pressure conditions.[13] For the Ba–C system, an open question is whether new compounds beyond BaC_2 and BaC_6 emerge upon increasing pressure. In this paper, we report the detailed high-pressure phase diagram of the Ba–C system based on our *ab initio* global variable-composition crystal structure search and discover a previously unknown metallic BaC phase that becomes stable at a remarkably low pressure of 3 GPa.

Computational details

Searches for stable structures were carried out using the USPEX code, based on the evolutionary algorithm[14–16] in the variable-composition

[a] *School of Materials Science and Engineering, Central South University, Changsha 410083, P. R. China*
[b] *Guangxi Key Laboratory of Information Materials, Guilin University of Electronic Technology, Guilin 541004, P. R. China. E-mail: chaohao.hu@guet.edu.cn*
[c] *International Center for Materials Physics, Chinese Academy of Sciences, Shenyang 110016, P. R. China*
[d] *Department of Geosciences, State University of New York, Stony Brook, NY 11794-2100, USA*
[e] *Center for Materials by Design, Institute for Advanced Computational Science, State University of New York, Stony Brook, NY 11794-2100, USA*
[f] *Moscow Institute of Physics and Technology, 9 Institutskiy lane, Dolgoprudny city, Moscow Region 141700, Russia*

mode. Many previous studies have demonstrated the power of this method/code in predicting stable crystal structures and novel compounds.[17–19] To explore all stable stoichiometric compounds and their crystal structures in the Ba–C binary system, we first performed the newly developed variable-composition searches (VCS)[20] and then focused on the most promising compositions using the traditional fixed-composition searches (FCS). Evolutionary predictions were performed at pressures 0, 10, 20, 30 and 40 GPa. During global optimization, a number of structures (with different compositions) are generated, relaxed, ranked on the basis of their fitness (which is derived from the computed energies). The underlying structure relaxations and total energy calculations were performed using the Vienna Ab-initio Simulation Package (VASP).[21] The projector augmented wave (PAW) method[22] was used to describe the interaction between core and valence electrons and the Perdew–Burke–Ernzerhof (PBE) implemented generalized gradient approximation[23] was used to treat the exchange–correlation energy. The valence electron configuration of Ba used here is $5s^2 5p^6 6s^2$. For structure relaxations, the plane-wave energy cutoff was set to be 540 eV and the Brillouin zone was sampled by uniform Γ-centered meshes with reciprocal-space resolution $2\pi \times 0.03$ A^{-1} or better.

The vibrational properties and electron–phonon coupling (EPC) coefficients were calculated by Quantum Espresso.[24] PBE-PAW atomic datasets were created with input data from PSLibrary.[25] These PAW potentials had the same valence electron configurations as the ones we used with the VASP code. Force constants were calculated using density-functional perturbation theory (DFPT).[26] In these calculations, we used a kinetic energy cutoff of 80 Ry, an $8 \times 8 \times 12$ k-point sampling mesh, a Gaussian smearing of 0.01 Ry, and a $4 \times 4 \times 6$ q-point mesh in the Brillouin zone for the newly-found BaC phase. The critical superconductivity temperature T_c was obtained from the Allen–Dynes modified McMillan equation.[27]

Results and discussion

Stability of compounds in multicomponent systems is defined by the convex hull construction. The calculated convex hulls for the Ba–C system at 0, 10, 20, 30, and 40 GPa are presented in Fig. 1. The well-known $P6_3/mmc$ (graphite) and $Fd\bar{3}m$ (diamond) phases of C, $Im\bar{3}m$ and $P6_3/mmc$ phases of Ba, and $P6_3/mmc$ BaC_6 intercalated compound can be reproduced readily in our searches. Remarkably, the previously reported compound BaC_2 never appears on the convex hull. According to the FCS simulations, we find that BaC_2 structure with space group $P\bar{1}$ at 0 GPa and *Cmcm* above 10 GPa are always more stable than the extensively studied tetragonal $I4/mmm$ and rhombohedral $R\bar{3}m$ phases of BaC_2 in the entire pressure range from 0 to 40 GPa. While the $P\bar{1}$ structure does have C_2 groups as in some dicarbides, the *Cmcm* phase of BaC_2 contains 1D gear-like chains of carbon atoms, being entirely different from the $I4/mmm$ and $R\bar{3}m$ phases in which the characteristic C_2 dumbbells are separate from each other. As shown in Fig. 1, however, it must be pointed out that none of the BaC_2 phases are stable at any pressure considered here.

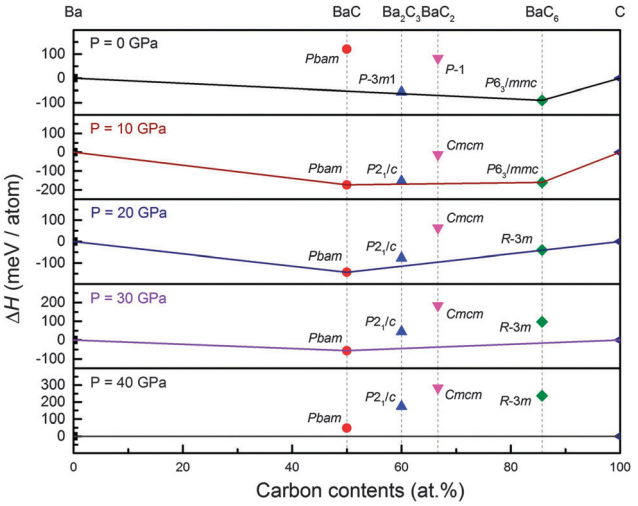

Fig. 1 Calculated convex hull diagrams of the Ba–C system at 0, 10, 20, 30, and 40 GPa.

Interestingly, from our VCS and FCS simulations at 10, 20, and 30 GPa, barium monocarbide (BaC) with space group *Pbam*, an unreported yet thermodynamically stable phase, is determined. As shown in Fig. 2(a), *Pbam*-BaC is a layered structure, in which layers of stoichiometry Ba_2C_3 alternate with pure Ba layers. In the "Ba_2C_3" layer, the linear C_3-groups and Ba atoms form characteristic Ba–C–C–C–Ba configuration, which is comparable to the layered Mg═C═C═C═Mg configuration in the experimentally determined magnesium sesquicarbide (Mg_2C_3) with space group *Pnnm*.[28] On the other hand, *Pbam*-BaC can be interpreted as a special structure in which the edge-sharing and distorted bcc-Ba columns, as marked in Fig. 2(b), form the basic framework intercalated by C_3-groups. It can be expected that these edge-sharing bcc-Ba building blocks would play an essential role in determining the electrical behavior of the *Pbam* phase. In fact, various Ba_2C_3 compounds, such as the intercalated $P\bar{3}m1$ phase containing the graphene sheets, *Pnnm* and $P2_1/c$ phases containing C_3-groups, were also detected from our FCS simulations at different pressures. As indicated in Fig. 1, however, Ba_2C_3 is always metastable. The optimized structural parameters of the *Pbam*

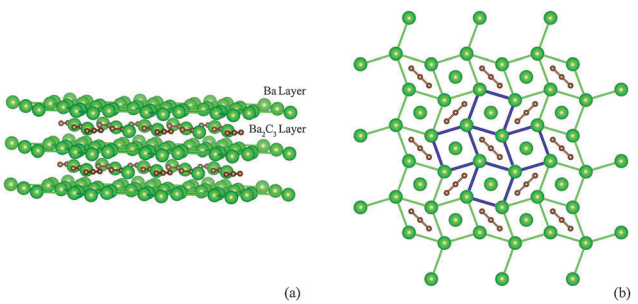

Fig. 2 Crystal structure of *Pbam*-BaC at 5 GPa: (a) side view with the marked "Ba_2C_3" and "Ba" atomic layers; (b) top view along the z axis in which the edge-sharing distorted bcc-Ba building blocks are marked in blue lines for clarity. Large green spheres and small brown spheres are Ba and C atoms, respectively.

Table 1 Optimized lattice parameters of the stable *Pbam* BaC at 5 GPa and metastable $P2_1/c$ (5 GPa), *Pnnm* (5 GPa), $P\bar{3}m1$ (5 GPa) phases of Ba_2C_3, $P\bar{1}$ (0 GPa) and *Cmcm* (5 GPa) phases of BaC_2

			Wyckoff positions				
Compound	Space group	Lattice parameters (Å, deg)	Atom	Site	x	y	z
BaC	*Pbam*	a = 7.650, b = 7.714, c = 4.428	Ba	2c	0.0000	1/2	0.0000
			Ba	4h	0.3425	0.3237	1/2
			C	2a	0.0000	0.0000	0.0000
			C	4g	0.1255	0.1212	0.0000
Ba_2C_3	$P2_1/c$	a = 4.314, b = 5.736, c = 7.763, β = 90.58	Ba	4e	0.2939	0.1284	0.6833
			C	2a	0.0000	0.0000	0.0000
			C	4e	0.1700	0.6808	0.5535
	Pnnm	a = 7.591, b = 6.803, c = 4.630	Ba	4g	0.2546	0.5447	1/2
			C	2b	0.0000	0.0000	1/2
			C	4g	0.0455	0.1901	1/2
	$P\bar{3}m1$	a = 4.344, c = 16.089	Ba	2c	0.0000	0.0000	1/3
			Ba	2d	1/3	2/3	0.1065
			C	6h	0.6671	0.6671	1/2
BaC_2	$P\bar{1}$	a = 4.467, b = 4.562, c = 8.200, α = 86.76, β = 105.00, γ = 64.47	Ba	2i	0.0479	0.6848	0.7485
			C	2i	0.6308	0.3743	0.5506
			C	2i	0.4550	0.0915	0.0532
	Cmcm	a = 4.408, b = 9.474, c = 4.887	Ba	4c	0.0000	0.3569	1/4
			C	8f	0.0000	0.0508	0.3911

BaC, the metastable $P\bar{3}m1$, *Pnnm*, and $P2_1/c$ phases of Ba_2C_3, and *Cmcm* of BaC_2 are listed in Table 1. At 5 GPa, the C–C bond lengths are about 1.330–1.341 Å in the structures containing C_3 groups, being longer than those of C_2 dumbbells – about 1.261–1.264 Å – in the *Cmcm*, *I4/mmm* or $R\bar{3}m$ BaC_2. This is consistent with C_2-dumbbells having a triple, and C_3-group double bonds.

The computed energetics of different phases has allowed us to construct the pressure-composition phase diagram of the Ba–C system, presented in Fig. 3. For pure C, the $P6_3/mmc$ graphite structure transforms into the cubic diamond structure with space group $Fd\bar{3}m$ at ~8 GPa, which is consistent with a great number of experimental or theoretical studies.[29,30] For pure Ba, the pressure-induced structural transition from $Im\bar{3}m$ to $P6_3/mmc$ is predicted to occur at ~3.5 GPa, which also agrees well with the previous experimental results or theoretical predictions.[31,32] At 14 GPa, the intercalated compound BaC_6 ($P6_3/mmc$) would lose its stability and transforms into a rhombohedral $R\bar{3}m$ phase, which is a CaC_6-type structure[1] and becomes unstable at 19 GPa. Above 3 GPa, *Pbam*-BaC becomes stable and coexists with Ba, C, and BaC_6. When pressure goes beyond 32 GPa, BaC finally decomposes into the $P6_3/mmc$ Ba and $Fd\bar{3}m$ C, and no Ba carbides remain stable. This pressure-induced decomposition in the Ba–C system has been observed in recent high-pressure X-ray diffraction and Raman spectroscopy measurements by Efthimiopoulos and co-authors,[10] where they suggested, however, that the irreversible amorphization above 30 GPa is due to decomposition of BaC_2.

The calculated electronic band structure and density of states (DOS) of the *Pbam* phase of BaC at 5 GPa are presented in Fig. 4. At 5 GPa, two bands which are marked as band I and band II in Fig. 4 cross the Fermi level (E_F), indicating metallic character of this phase. Band I makes two small hole-pockets along the Γ–Z–U path, while band II makes an electron-pocket around the Γ point. Moreover, the total DOS at E_F is about

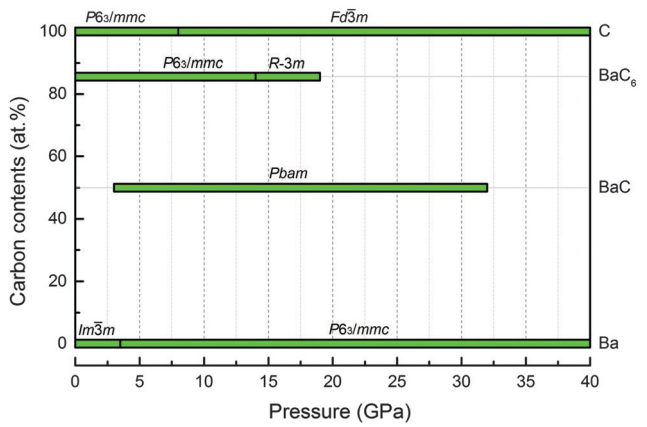

Fig. 3 Pressure-composition phase diagram of the Ba–C system.

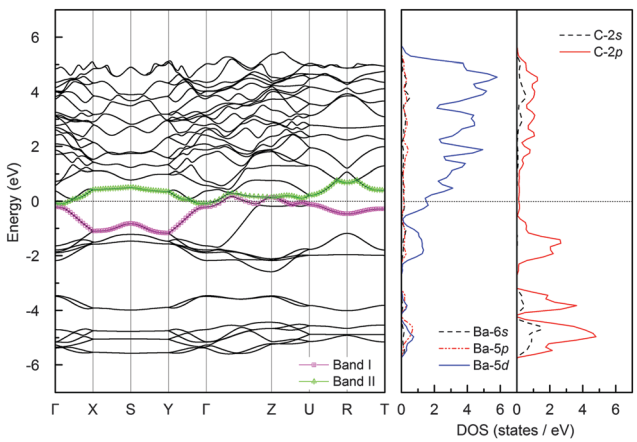

Fig. 4 Band structure along high-symmetry lines in the Brillion zone and projected electronic density of states of the *Pbam* phase of BaC at 5 GPa.

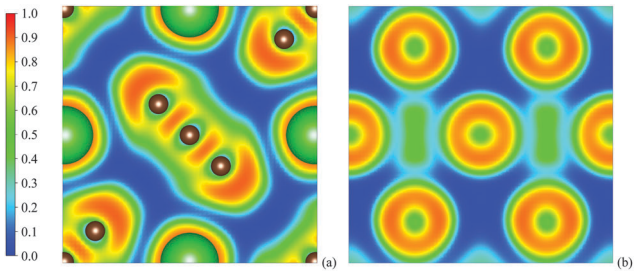

Fig. 5 2D slices of electron localization function for the *Pbam* phase of BaC at 5 GPa: (a) ELF for the (001) plane through the C_3 group and Ba atoms; (b) ELF for the plane through Ba atoms.

0.71 states per eV per f.u., which is mainly contributed by the Ba-5d states and to a small extent also the C-2p states. When pressure goes up to 15 GPa, the total DOS is broadened considerably, but band I makes only one hole-pocket and the DOS at E_F drops to about 0.42 states per eV per f.u., indicating the decrease of conductivity.

Fig. 5 shows the calculated electron localization function (ELF) of *Pbam*-BaC at 5 GPa. As presented in Fig. 5(a), the ELF values between carbon atoms in the C_3 group are nearly 1.0, indicating strong covalent bonding. The ELF value between the nearest Ba atoms, as shown in Fig. 5(b), is about 0.5, indicating metallic bonding among them, which is consistent with our previous analysis of the crystal structure and electronic DOS.

The calculated phonon dispersion curves along high-symmetry directions in the Brillion zone, projected phonon DOS, and Eliashberg spectral function α^2F with the integral curve of the electron–phonon coupling parameter λ for *Pbam*-BaC at 5 GPa are shown in Fig. 6. The dynamical stability of the *Pbam* phase is confirmed by the absence of imaginary frequencies. The low-frequency vibrations below 130 cm^{-1} are mainly contributed by the heavy Ba atoms, but the coupled Ba–C translational motions are also not negligible. In the higher-frequency region between 171 and 275 cm^{-1}, the phonon spectrum is mainly due to the librational motions of C_3 groups. The two flat bands at around 585 and 609 cm^{-1} can be assigned to the bending vibrations of the linear C_3 groups. The phonon modes at around 1127 cm^{-1} correspond to stretching of bonds between the C(2a) and C(4g) atoms in C_3 groups, but do not contain a displacement of the central C(2a) atom due to symmetry. At high frequencies above 1687 cm^{-1}, the phonon spectrum is mainly ascribed to the stretching vibrations between C(4g) atoms and C(2a)–C(4g) pairs in C_3 groups. In addition, according to our phonon calculations at 0 GPa, the *Pbam* BaC is still dynamically stable, which indicates that this compound may be quenchable under normal conditions.

The calculated Eliashberg spectral function $\alpha^2F(\omega)$ of BaC under 5 GPa is depicted in Fig. 6. The corresponding integral of EPC parameter $\lambda(\omega)$ is about 0.65, indicating a moderate EPC strength. The vibrations below 130 cm^{-1} mostly from Ba atoms contribute about 60.0% of the total λ value. The librational vibrations of C_3 groups within the 171–275 cm^{-1} frequency range contribute about 29.7%, while about 4.9% and 4.6% of the total λ are from the bending motions of C_3 groups between 585 and 609 cm^{-1} and the stretching vibrations of C atoms above 1687 cm^{-1}, respectively. The calculated logarithmic average frequency ω_{log} is relatively low – 151.1 K at a pressure of 5 GPa. The corresponding critical superconductivity temperature T_c, obtained from the modified Allen–Dynes equation using commonly accepted Coulomb pseudopotential, $\mu^* = 0.10$, is about 4.32 K. Moreover, this value of T_c is somewhat higher than that of the pure metallic Ba (<1.3 K at the pressure of 5.5 GPa), which verifies that the contributions of the vibrations of C_3 groups to the superconducting behavior of the *Pbam* BaC cannot be ignored. With increasing pressure, the calculated T_c drops to 1.54 K at 10 GPa, and 0.76 K at 15 GPa due to the weaker EPC strength. This is in contrast to the case of pure Ba, where T_c increases with pressure.[33] Similar behavior, however, appears in many phonon-mediated superconductors, such as the extensively studied MgB_2,[34] CaC_6,[35] and BH recently reported by us.[36]

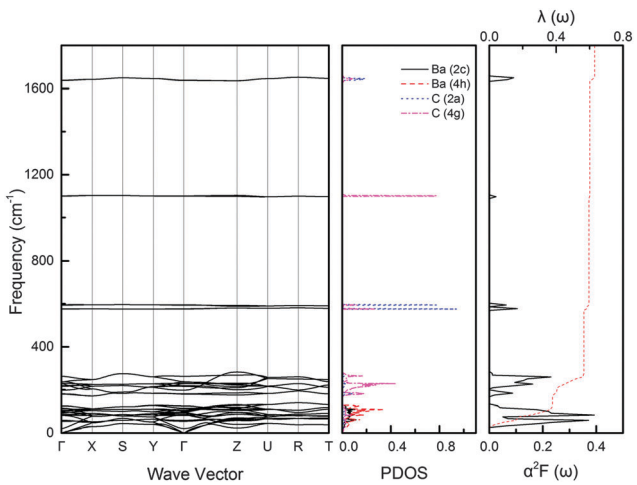

Fig. 6 Calculated phonon dispersion, projected phonon density of states and Eliashberg spectral function α^2F with the integral curve of the electron–phonon parameter λ.

Conclusions

A high-pressure phase diagram of the Ba–C system built from first-principle total-energy calculations and *ab initio* evolutionary structure prediction simulations has indicated that at 0 K the extensively studied barium dicarbide (BaC_2) is always metastable. According to our evolutionary structure searches and static enthalpy-pressure calculations, barium monocarbide (BaC) with space group *Pbam* is found to be stable in the pressure range from 3.1 to 32.3 GPa. BaC finally decomposes into Ba and C above 32.3 GPa, which is consistent with the recent experimental work. Unlike BaC_2 containing C_2 dumbbells, the orthorhombic *Pbam*-BaC has the characteristic linear three-membered carbon C_3-groups. *Pbam*-BaC is metallic with mostly Ba-5d states at the Fermi level. Electronic structure calculations also show strong covalent bonding within C_3-groups in the *Pbam* phase. Lattice dynamics and electron–phonon coupling calculations further indicate that the *Pbam* phase is

a phonon-mediated superconductor with a moderate EPC strength and T_c = 4.32 K at 5 GPa.

Acknowledgements

We gratefully acknowledge the financial support from the National Basic Research Program of China (973 Program, Grant No. 2014CB643703), the National Natural Science Foundation of China (Grant No. 11164005 and No. 51371061), the Guangxi Natural Science Foundation (Grant No. 2014GXNSFGA118001 and No. 2012GXNSFGA060002), and Guangxi Key Laboratory of Information Materials (Grant No. 1210908-215-Z), National Science Foundation (EAR-1114313, DMR-1231586), DARPA (Grant No. W31P4Q1210008 and No. W31P4Q1310005), the Government (No. 14.A12.31.0003) and the Ministry of Education and Science of Russian Federation (Project No. 8512), and Foreign Talents Introduction and Academic Exchange Program (No. B08040). The authors also acknowledge the High Performance Computing Center of Guilin University of Electronic Technology.

References

1 N. Emery, C. Herold, M. d'Astuto, V. Garcia, C. Bellin, J. F. Mareche, P. Lagrange and G. Loupias, *Phys. Rev. Lett.*, 2005, **95**, 087003.
2 T. E. Weller, M. Ellerby, S. S. Saxena, R. P. Smith and N. T. Skipper, *Nat. Phys.*, 2005, **1**, 39–41.
3 T. Gulden, R. W. Henn, O. Jepsen, R. K. Kremer, W. Schnelle, A. Simon and C. Felser, *Phys. Rev. B: Condens. Matter Mater. Phys.*, 1997, **56**, 9021–9029.
4 V. Babizhetskyy, O. Jepsen, R. K. Kremer, A. Simon, B. Ouladdiaf and A. Stolovits, *J. Phys.: Condens. Matter*, 2014, **26**, 025701.
5 Y. Koike, H. Suematsu, K. Higuchi and S. Tanuma, *Physica B+C*, 1980, **99**, 503–508.
6 I. T. Belash, A. D. Bronnikov, O. V. Zharikov and A. V. Pal'nichenko, *Solid State Commun.*, 1989, **69**, 921–923.
7 I. T. Belash, A. D. Bronnikov, O. V. Zharikov and A. V. Palnichenko, *Solid State Commun.*, 1987, **64**, 1445–1447.
8 G. Csányi, P. B. Littlewood, A. H. Nevidomskyy, C. J. Pickard and B. D. Simons, *Nat. Phys.*, 2005, **1**, 42–45.
9 X. Blase, E. Bustarret, C. Chapelier, T. Klein and C. Marcenat, *Nat. Mater.*, 2009, **8**, 375–382.
10 I. Efthimiopoulos, K. Kunc, G. V. Vazhenin, E. Stavrou, K. Syassen, M. Hanfland, S. Liebig and U. Ruschewitz, *Phys. Rev. B: Condens. Matter Mater. Phys.*, 2012, **85**, 054105.
11 J. Feng, B. Xiao and J. Chen, *Sci. China, Ser. B: Chem.*, 2008, **51**, 545–550.
12 S. Nakamae, A. Gauzzi, F. Ladieu, D. L'Hôte, N. Eméry, C. Hérold, J. F. Marêché, P. Lagrange and G. Loupias, *Solid State Commun.*, 2008, **145**, 493–496.
13 R. J. Hemley and N. W. Ashcroft, *Phys. Today*, 1998, **51**, 26.
14 A. R. Oganov and C. W. Glass, *J. Chem. Phys.*, 2006, **124**, 244704.
15 A. R. Oganov, A. O. Lyakhov and M. Valle, *Acc. Chem. Res.*, 2011, **44**, 227–237.
16 A. R. Oganov, Y. Ma, A. O. Lyakhov, M. Valle and C. Gatti, *Rev. Mineral. Geochem.*, 2010, **71**, 271–298.
17 A. R. Oganov, J. Chen, C. Gatti, Y. Ma, Y. Ma, C. W. Glass, Z. Liu, T. Yu, O. O. Kurakevych and V. L. Solozhenko, *Nature*, 2009, **457**, 863–867.
18 Y. Ma, M. Eremets, A. R. Oganov, Y. Xie, I. Trojan, S. Medvedev, A. O. Lyakhov, M. Valle and V. Prakapenka, *Nature*, 2009, **458**, 182–185.
19 W. Zhang, A. R. Oganov, A. F. Goncharov, Q. Zhu, S. E. Boulfelfel, A. O. Lyakhov, E. Stavrou, M. Somayazulu, V. B. Prakapenka and Z. Konôpková, *Science*, 2013, **342**, 1502–1505.
20 A. O. Lyakhov, A. R. Oganov, H. T. Stokes and Q. Zhu, *Comput. Phys. Commun.*, 2013, **184**, 1172–1182.
21 G. Kresse and J. Furthmüller, *Phys. Rev. B: Condens. Matter Mater. Phys.*, 1996, **54**, 11169–11186.
22 P. E. Blochl, *Phys. Rev. B: Condens. Matter Mater. Phys.*, 1994, **50**, 17953–17979.
23 J. P. Perdew, K. Burke and M. Ernzerhof, *Phys. Rev. Lett.*, 1996, **77**, 3865–3868.
24 G. Paolo, B. Stefano, B. Nicola, C. Matteo, C. Roberto, C. Carlo, C. Davide, L. C. Guido, C. Matteo, D. Ismaila, C. Andrea Dal, G. Stefano de, F. Stefano, F. Guido, G. Ralph, G. Uwe, G. Christos, K. Anton, L. Michele, M.-S. Layla, M. Nicola, M. Francesco, M. Riccardo, P. Stefano, P. Alfredo, P. Lorenzo, S. Carlo, S. Sandro, S. Gabriele, P. S. Ari, S. Alexander, U. Paolo and M. W. Renata, *J. Phys.: Condens. Matter*, 2009, **21**, 395502.
25 A. D. Corso, *PSLibrary, 0.3.1 edn.*, 2013.
26 S. Baroni, S. de Gironcoli, A. Dal Corso and P. Giannozzi, *Rev. Mod. Phys.*, 2001, **73**, 515–562.
27 P. B. Allen and R. C. Dynes, *Phys. Rev. B: Solid State*, 1975, **12**, 905–922.
28 H. Fjellvaag and P. Karen, *Inorg. Chem.*, 1992, **31**, 3260–3263.
29 H. Hirai, K. Kondo and T. Ohwada, *Carbon*, 1995, **33**, 203–208.
30 S. Scandolo, M. Bernasconi, G. L. Chiarotti, P. Focher and E. Tosatti, *Phys. Rev. Lett.*, 1995, **74**, 4015–4018.
31 T. Kenichi, *Phys. Rev. B: Condens. Matter Mater. Phys.*, 1994, **50**, 16238–16246.
32 S. K. Reed and G. J. Ackland, *Phys. Rev. Lett.*, 2000, **84**, 5580–5583.
33 J. Wittig and B. T. Matthias, *Phys. Rev. Lett.*, 1969, **22**, 634–636.
34 J. Nagamatsu, N. Nakagawa, T. Muranaka, Y. Zenitani and J. Akimitsu, *Nature*, 2001, **410**, 63–64.
35 M. Debessai, J. J. Hamlin, J. S. Schilling, D. Rosenmann, D. G. Hinks and H. Claus, *Phys. Rev. B: Condens. Matter Mater. Phys.*, 2010, **82**, 132502–132504.
36 C. H. Hu, A. R. Oganov, Q. Zhu, G. R. Qian, G. Frapper, A. O. Lyakhov and H. Y. Zhou, *Phys. Rev. Lett.*, 2013, **110**, 165504.

